AIAA JOURNAL
Vol. 40, No. 8, August 2002

Simultaneous Modeling of Mechanical and Electrical Response of Smart Composite Structures

Robert P. Thornburgh* and Aditi Chattopadhyay†
Arizona State University, Tempe, Arizona 85287-6106

A smart structural model is developed to determine analytically the response of arbitrary structures with piezoelectric materials and attached electrical circuitry. The equations of motion are formulated using the coupled piezoelectric formulations. However, rather than solving for strain and electric field, the proposed model solves for the strain and electric charge. The equations of motion are simplified for the case of a composite plate structure using a refined higher-order laminate theory; however, the model is applicable to most structural models. Additional degrees of freedom are then added to describe any attached electrical circuitry. A method is also presented for system simplification using the structural mode shapes and natural frequencies. Results are verified using experimental data for passive electrical shunt damping. The developed model results in a general framework that can be useful in solving a wide variety of coupled piezoelectric–mechanical problems addressing issues such as passive electrical damping, self-sensing, and electrical power consumption.

Nomenclature

A	=	total lead zirconate titanate piezoelectric device (PZT) in-plane area
$\boldsymbol{A}_q$	=	electric displacement to total charge relation
$\boldsymbol{B}$	=	dielectric permitivity matrix
c_{ijkl}	=	elastic constants
$D_i, \boldsymbol{D}$	=	electric displacement vector
$\boldsymbol{D}_e$	=	nodal electric displacement vector
$E_I, \boldsymbol{E}$	=	electric field vector
e_{ijk}	=	piezoelectric constants
$\boldsymbol{f}_B, \boldsymbol{f}_S$	=	body forces and surface tractions
$\boldsymbol{H}$	=	electric enthalpy
h	=	laminate thickness
k_{ij}	=	dielectric permitivity constants
$\boldsymbol{L}_u$	=	mechanical displacement operator matrix
$\boldsymbol{L}_\varepsilon$	=	displacement to strain operator matrix
$\boldsymbol{N}_q$	=	interpolation matrix for charge density
$\boldsymbol{N}_u$	=	interpolation matrix for mechanical displacement
$\boldsymbol{P}$	=	piezoelectric coupling matrix
$\boldsymbol{Q}$	=	stress–strain relation matrix
q	=	total PZT charge
$\boldsymbol{r}$	=	modal contribution for reduced system
u, v, w	=	mechanical displacements along x, y, z directions
$\boldsymbol{u}_e$	=	nodal displacement vector
z	=	location relative to laminate midplane
γ	=	material damping coefficient
$\varepsilon_{ij}, \varepsilon$	=	strain tensor and engineering strain vector
μ_m	=	modal damping coefficient
ρ	=	density
σ_{ij}, σ	=	stress tensor and stress vector
Φ	=	modal matrix
ϕ	=	electric potential
φ	=	open circuit eigenvector
ψ_x, ψ_y	=	rotations of the normals to midplane about y and x axes
ω	=	natural frequency

Received 27 March 2001; revision received 6 August 2001; accepted for publication 21 April 2002.

*Graduate Research Assistant, Department of Mechanical and Aerospace Engineering. Student Member AIAA.

†Professor, Department of Mechanical and Aerospace Engineering. Associate Fellow AIAA.

I. Introduction

THE interaction between structural characteristics and associated electrical circuitry is an often overlooked aspect of smart structural systems. Piezoelectric actuators are often used to control the dynamic response of structures; however, the dynamic response of the structure is modified by the addition of these actuators. The lead zirconate titanate piezoelectric device (PZT) or other piezoelectric material adds additional stiffness to the structure, but this stiffness is dependent on the electrical circuitry attached to each PZT. This can be easily seen in the simple comparison between actuators that are open circuited and those that are shorted out. Under structural deflection, potential energy is stored in the PZT in the form of mechanical strain and also electrical potential similar to a capacitor. When the PZT has been shorted out by having its electrodes connected, electrical potential can no longer be stored. This reduction in the system's ability to store energy results in a reduction in the effective stiffness of the system. The magnitude of this reduction is dependent on the piezoelectric material's dielectric permitivity, or capacitance, relative to its piezoelectric properties. In more practical examples, this coupling is encountered in the interaction between the structural stiffness and the electrical potential resulting from a combination of mechanical and electrical loading. When piezoelectric constants are experimentally determined, the PZT is usually unconstrained. When applied to a structure, the PZT is no longer able to deform to its unconstrained shape when a voltage is applied. This change in the strain field causes a reduction in the electrical potential stored in the PZT and, thus, a smaller actuation force than that predicted using an uncoupled theory based on the unconstrained piezoelectric constants. For this reason, piezoelectric manufacturers often list both free and clamped, as well as shorted and open circuited, material properties for PZT. However, a PZT mounted to a flexible structure is neither free nor clamped, and so arbitrary use of the manufacturer values can lead to analytic errors during structural modeling. If the piezoelectric–mechanical coupling effects are taken into account, then it is no longer necessary to identify these separate parameters.

A description of the electrical interaction with the structural deformation also allows numerous other applications such as modeling of passive electrical damping systems[1–6] and self-sensing actuators,[7] as well as analytical determination of power consumption. Hagood and Von Flotow[1] and Hagood and Crawley[2] conducted a large amount of work in the areas of passive electrical damping and self-sensing actuators[7] using coupled equations similar to those used in this work. However, the elegant electrical models relied on a comparatively simple description of the strain field in the piezoelectric material, and analytical modeling of specific structures contained noticeable errors as a result of the approximations used. Most structural models utilizing piezoelectric actuators

rely on an uncoupled approach, where the effects of applied voltage are treated as loads and the electrical equations are not used, as was done by Crawley[8] and Detwiler et al.[9] This precludes their effective use in solving for the electrical effects on structural response. A general two-way coupled theory was introduced in the hybrid plate theory developed by Mitchell and Reddy.[10] In this model, a mathematical description of the electric potential was assumed and could be solved for simultaneously with mechanical displacements. This concept was extended by using a refined higher-order plate theory and coupled to the thermal field by Chattopadhyay et al.[11] The description of the electrical potential was then improved by using a third-order function of the through-the-thickness coordinate by Zhou et al.[12] This model allowed for conservation of charge across the PZT and showed the interaction of bending strains with the electrical field within the piezoelectric material. The disadvantage of these models is that additional degrees of freedom are added to the system to describe the distribution of electrical potential (and, thus, the electric field) within each PZT. The number of degrees of freedom increases with the PZT area and level of finite element mesh refinement. Also, the resulting system of equations is no longer symmetric positive definite, which adds to the computational effort.

Thus, the objective of this research is to develop a model that can be utilized to solve simultaneously for the response of a system composed of base structure, piezoelectric materials, and electrical components. Instead of assuming a description of the electric potential within the PZT, the model provides an accurate description of the charge within the PZT by using a constant value for the electric displacement through the thickness of the piezoelectric material. For the case of small PZTs in uniform strain fields, the electric charge can be considered evenly distributed over the surface electrode; thus, a single degree of freedom, normally electrode charge, is added for each PZT. This model also results in the voltage being applied as an external load on the electrical portion of the system. The resulting model has the advantage that it can be applied to any plate theory such as classical, first order, or higher order, with the addition of only a single degree of freedom per PZT. Also, the resulting system of equations is symmetric positive definite, minimizing the computational effort associated with the analysis of smart structural systems.

II. Mathematical Formulation

A. Equations of Motion

The construction of a model for smart composite laminates starts with the formulation of the constitutive relations. The potential energy contained in a piezoelectric medium can be described by a function called the electric enthalpy density function H. Traditionally this is expressed as a function of the components of strain ε_{ij} and electric field E_i as follows:

$$H(\varepsilon_{ij}, E_i) = \tfrac{1}{2}c_{ijkl}\varepsilon_{ij}\varepsilon_{kl} - e_{ijk}E_i\varepsilon_{jk} - \tfrac{1}{2}k_{ij}E_iE_j \tag{1}$$

This potential function leads to the familiar equations

$$\sigma_{ij} = \frac{\partial H(\varepsilon_{ij}, E_i)}{\partial \varepsilon_{ij}} = c_{ijkl}\varepsilon_{kl} - e_{ijk}E_k \tag{2}$$

$$D_i = -\frac{\partial H(\varepsilon_{ij}, E_i)}{\partial E_i} = e_{ijk}\varepsilon_{jk} + k_{ij}E_j \tag{3}$$

where σ_{ij} and D_i are the components of the mechanical stress and the electrical displacement, respectively. Note that the elastic constants used are the zero electric field values (PZT is shorted out) and that the dielectric permitivities are the zero strain values (clamped). In matrix form, these equations can be written as follows:

$$\boldsymbol{\sigma} = \boldsymbol{Q}\boldsymbol{\varepsilon} - \boldsymbol{P}\boldsymbol{E} \tag{4}$$

$$\boldsymbol{D} = \boldsymbol{P}^T\boldsymbol{\varepsilon} + \boldsymbol{B}\boldsymbol{E} \tag{5}$$

Equation (2) is often referred to as the converse effect, and Eq. (3) is known as the direct effect. These equations are traditionally used due to the ease with which piezoelectric materials can be modeled as either actuators or sensors. The electric field, a function of the electrical potential ϕ, is defined as

$$E_i = -\frac{\partial \phi}{\partial x_i} \tag{6}$$

Most formulations make the assumption, based on the geometry of thin, electroded piezoelectrics, that the electric field is constant through the thickness of the material and zero within the plane of the piezoelectric. This in turn specifies that the electric field can be simply expressed as

$$E_3 = -(V/t_{\text{pzt}}) \tag{7}$$

where V is the difference in voltage across the upper and lower electrodes and t_{pzt} is the thickness of the piezoelectric material. The piezoelectric material can be used as an actuator by the use of Eq. (2) with the applied voltage creating a known stress or force on the structure. Sensors can be modeled using Eq. (3) and the strain in the deformed structure to create an output voltage. This type of technique, where the equations are solved sequentially, is an uncoupled approach, and it does not take into account the full interaction between the strain field and the electric field. A coupled approach like that used by Hagood and Von Flotow[1] as well as Mitchell and Reddy[10] is to solve Eqs. (2) and (3) simultaneously, thus ensuring that both equations are satisfied. Note, however, that if the strain is not constant through the thickness of the piezoelectric material, such as in the case of bending or transverse shear, then this method results in electric displacement varying through the thickness. This also implies differing amounts of charge on the upper and lower electrodes, which is a violation of the conservation of charge. This has been resolved by making the electric potential, and in turn the electric field, higher-order functions of the through-the-thickness coordinate to match the displacement and strain fields in the structure. However, such an approach leads to additional degrees of freedom to describe the electric potential. Another drawback is that the resulting system matrices in finite element implementation are not symmetric. This results in a sizable increase in the computational effort required to solve the system of equations.

To address these issues, a different approach is used in the current work. Equations (4) and (5) are reformulated in terms of the mechanical strain and the electric displacement as follows:

$$\boldsymbol{\sigma} = (\boldsymbol{Q} + \boldsymbol{P}\boldsymbol{B}^{-1}\boldsymbol{P}^T)\boldsymbol{\varepsilon} - (\boldsymbol{P}\boldsymbol{B}^{-1})\boldsymbol{D} \tag{8}$$

$$\boldsymbol{E} = -(\boldsymbol{B}^{-1}\boldsymbol{P}^T)\boldsymbol{\varepsilon} + \boldsymbol{B}^{-1}\boldsymbol{D} \tag{9}$$

In this formulation, the increase in stiffness caused by open circuiting the piezoelectric ($\boldsymbol{D} = 0$) can easily be seen, and $\boldsymbol{Q} + \boldsymbol{P}\boldsymbol{B}^{-1}\boldsymbol{P}^T$ represents the open circuit stiffness. When this formulation is used, the electric displacement $\boldsymbol{D}$ can be taken as constant through the thickness of the PZT, thus ensuring conservation of charge on each of the electrodes. If the PZT is assumed to have its entire upper and lower surfaces covered by electrodes, then the electric displacement is constant through the thickness of the PZT. If the PZT is relatively small compared to the base structure, which is often the case in practical applications, and the strain over the surface of the PZT is relatively uniform, then the electrical displacement can be assumed to be constant across the entire PZT, meaning that the surface charge is uniformly distributed. In that case, only one unknown per PZT is added to the system of equations. For structures with larger PZTs, larger strain gradients, or when greater accuracy is desired, the electrical displacement can be discretized using a finite element mesh. Another advantage of this formulation is that applied voltage now appears as an applied electrical load, similar to an applied mechanical traction. The electric enthalpy expressed in terms of strain and electric displacement now takes the form

$$\boldsymbol{H}(\boldsymbol{\varepsilon}, \boldsymbol{D}) = \tfrac{1}{2}\boldsymbol{\varepsilon}^T(\boldsymbol{Q} + \boldsymbol{P}\boldsymbol{B}^{-1}\boldsymbol{P}^T)\boldsymbol{\varepsilon} - \boldsymbol{\varepsilon}^T\boldsymbol{P}\boldsymbol{B}^{-1}\boldsymbol{D} + \tfrac{1}{2}\boldsymbol{D}^T\boldsymbol{B}^{-1}\boldsymbol{D} \tag{10}$$

The equations of motion can be formed using a variational approach and Hamilton's principle similar to that by Tiersten.[13] The variation principle from time t_0 to t for the piezoelectric body, V, can be written as follows:

$$\delta\Pi = 0 = \int_{t_0}^{t}\int_{V}\left[\delta\left(\frac{1}{2}\rho\dot{\boldsymbol{u}}^T\dot{\boldsymbol{u}}\right) - \delta\boldsymbol{H}(\boldsymbol{\varepsilon}, \boldsymbol{D})\right]\mathrm{d}V\,\mathrm{d}t + \int_{t_0}^{t}\delta\boldsymbol{W}\,\mathrm{d}t \tag{11}$$

where the first term represents the kinetic energy, the second term the electric enthalpy, and $\delta \boldsymbol{W}$ is the total virtual work done on the structure. The term $\boldsymbol{u}$ is the mechanical displacement. The work done by body forces $\boldsymbol{f}_B$, surface tractions $\boldsymbol{f}_S$ and electrical potential ϕ applied to the surface of the piezoelectric material can be expressed by

$$\delta \boldsymbol{W} = \int_V \delta \boldsymbol{u}^T \boldsymbol{f}_B \, \mathrm{d}V + \int_S \delta \boldsymbol{u}^T \boldsymbol{f}_S \, \mathrm{d}S + \int_S \delta \boldsymbol{D}^T \phi \, \mathrm{d}S \tag{12}$$

Equations (10–12) provide the equations of motion for the piezoelectric body. To solve them, assumptions must be made concerning the nature of the mechanical strain and the electrical displacement.

B. Finite Element Formulation

Assumptions are made that the piezoelectric material is oriented with its polarization axis normal to the plane of the plate and that the PZT has electrodes covering its upper and lower surfaces. This is the usual geometry for transversely operating piezoelectric actuators and sensors bonded to or embedded in plate structures. For this case, the electric displacement becomes

$$\boldsymbol{D}_1 = \boldsymbol{D}_2 = 0 \tag{13a}$$

and for small PZTs

$$\boldsymbol{D}_3 = \frac{\partial q}{\partial A} \approx \frac{q}{A} \tag{13b}$$

where q is the amount of positive charge on the lower electrode and A is the surface area of the PZT electrode. For the case of small PZTs, Eq. (11) is reduced to

$$\int_{t_0}^{t} \int_V \left[\delta \left(\frac{1}{2} \rho \dot{\boldsymbol{u}}^T \dot{\boldsymbol{u}} \right) - \delta \varepsilon^T (\boldsymbol{Q} + \boldsymbol{P}\boldsymbol{B}^{-1}\boldsymbol{P}^T)\varepsilon + \delta \varepsilon^T \boldsymbol{P}\boldsymbol{B}^{-1} \begin{Bmatrix} 0 \\ 0 \\ 1 \end{Bmatrix} \frac{q}{A} \right.$$

$$\left. + \frac{\delta q}{A} \begin{Bmatrix} 0 \\ 0 \\ 1 \end{Bmatrix}^T \boldsymbol{B}^{-1}\boldsymbol{P}^T \varepsilon - \frac{\delta q q}{b_{33} A^2} \right] \mathrm{d}V \, \mathrm{d}t$$

$$+ \int_{t_0}^{t} \left\{ \int_V \delta \boldsymbol{u}^T \boldsymbol{f}_B \, \mathrm{d}V + \int_S \delta \boldsymbol{u}^T \boldsymbol{f}_S \, \mathrm{d}S + \delta q \phi \right\} \mathrm{d}t = 0 \tag{14}$$

If the assumption of uniform charge distribution over the surface of the PZT is not considered valid, due to the presence of a large strain gradient across the PZT, or if greater accuracy is desired, then the electric displacement can be discretized using a finite element mesh. The electric displacement then becomes

$$\frac{\partial q}{\partial A} = \boldsymbol{N}_q(\boldsymbol{x}, \boldsymbol{y}) \left(\frac{\partial q}{\partial A} \right)_e \tag{15}$$

where $(\partial \boldsymbol{q}/\partial \boldsymbol{A})_e$ is the nodal electrical displacement and $\boldsymbol{N}_q(\boldsymbol{x}, \boldsymbol{y})$ is the interpolation matrix. Equation (11) now becomes

$$\int_{t_0}^{t} \int_V \left[\delta \left(\frac{1}{2} \rho \dot{\boldsymbol{u}}^T \dot{\boldsymbol{u}} \right) - \delta \varepsilon^T (\boldsymbol{Q} + \boldsymbol{P}\boldsymbol{B}^{-1}\boldsymbol{P}^T)\varepsilon \right.$$

$$+ \delta \varepsilon^T \boldsymbol{P}\boldsymbol{B}^{-1} \begin{Bmatrix} 0 \\ 0 \\ 1 \end{Bmatrix} \boldsymbol{N}_q \left(\frac{\partial q}{\partial A} \right)_e + \delta \left(\frac{\partial q}{\partial A} \right)_e^T \boldsymbol{N}_q^T \begin{Bmatrix} 0 \\ 0 \\ 1 \end{Bmatrix}^T \boldsymbol{B}^{-1}\boldsymbol{P}^T \varepsilon$$

$$\left. - \frac{1}{b_{33}} \delta \left(\frac{\partial q}{\partial A} \right)_e^T \boldsymbol{N}_q^T \boldsymbol{N}_q \left(\frac{\partial q}{\partial A} \right)_e \right] \mathrm{d}V \, \mathrm{d}t$$

$$+ \int_{t_0}^{t} \left\{ \int_V \delta \boldsymbol{u}^T \boldsymbol{f}_B \, \mathrm{d}V + \int_S \delta \boldsymbol{u}^T \boldsymbol{f}_S \, \mathrm{d}S + \delta q \phi \right\} \mathrm{d}t = 0 \tag{16}$$

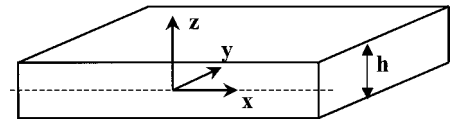

Fig. 1 Plate geometry and coordinate system.

A refined higher-order laminate theory developed by Reddy[14,15] is used to model the mechanical displacement field. The body is assumed to be a plate structure composed of an arbitrary number of orthotropic lamina arranged with varying orientations. The coordinate system for the plate is taken to be with the x–y plane parallel to the plane of the plate and the z coordinate normal to the plane of the plate measured from the center of thickness (Fig. 1). The refined higher-order theory assumes a parabolic distribution of transverse shear strain, thus providing accurate estimation of transverse shear stresses for moderately thick constructions with little increase in computational effort. The theory starts with a general third-order displacement field and is simplified by imposing the stress free boundary conditions on the free surfaces. Because the laminate is orthotropic, this implies that the transverse shear strains are zero. The refined displacement field now takes the following form:

$$\boldsymbol{u}_1 = u + z\left(\psi_x - \frac{\partial w}{\partial x} \right) - \frac{4z^3}{3h^2} \psi_x \tag{17a}$$

$$\boldsymbol{u}_2 = v + z\left(\psi_y - \frac{\partial w}{\partial y} \right) - \frac{4z^3}{3h^2} \psi_y \tag{17b}$$

$$\boldsymbol{u}_3 = w \tag{17c}$$

where u, v, and w are the displacements of the midplane and ψ_x and ψ_y are the rotations of the normal at $z = 0$ about the $-y$ and $-x$ axes, respectively. Note that u, v, w, ψ_x, and ψ_y are all functions of the x and y coordinates only. The variable z represents the location with respect to the midplane of the plate, and h is the total plate thickness.

When the preceding equations are used, the equations of motion can be simplified by the reduction of the mechanical displacements and strains to the variables u, v, w, ψ_x, and ψ_y. The displacement vector $\boldsymbol{u}$ and the strain vector ε can be written using a finite element formulation as follows:

$$\boldsymbol{u} = \boldsymbol{L}_u \boldsymbol{u}_u, \qquad \varepsilon = \boldsymbol{L}_\varepsilon \boldsymbol{u}_u \tag{18}$$

where

$$\boldsymbol{u}_u = \boldsymbol{N}_u(x, y) \boldsymbol{u}_e \tag{19}$$

with $\boldsymbol{u}_u$ the displacement field vector, $\boldsymbol{u}_e$ the nodal displacement vector, and $\boldsymbol{N}_u(x, y)$ an interpolation matrix.

When it is assumed that the smart structure contains n small PZTs, the equations of motion become

$$\int_{t_0}^{t} \int_V \left[\delta \boldsymbol{u}_e^T \boldsymbol{N}_u^T \boldsymbol{L}_u^T \rho \boldsymbol{L}_u \boldsymbol{N}_u \ddot{\boldsymbol{u}}_e \right.$$

$$\left. + \delta \boldsymbol{u}_e^T \boldsymbol{N}_u^T \boldsymbol{L}_\varepsilon^T (\boldsymbol{Q} + \boldsymbol{P}\boldsymbol{B}^{-1}\boldsymbol{P}^T) \boldsymbol{L}_\varepsilon \boldsymbol{N}_u \boldsymbol{u}_e \right] \mathrm{d}V \, \mathrm{d}t$$

$$+ \sum_{i=1}^{n} \int_{t_0}^{t} \int_V \left[-\delta \boldsymbol{u}_e^T \boldsymbol{N}_u^T \boldsymbol{L}_\varepsilon^T \boldsymbol{P}\boldsymbol{B}^{-1} \begin{Bmatrix} 0 \\ 0 \\ 1 \end{Bmatrix} \frac{q_i}{A_i} - \frac{\delta q_i}{A_i} \begin{Bmatrix} 0 \\ 0 \\ 1 \end{Bmatrix}^T \right.$$

$$\left. \times \boldsymbol{B}^{-1}\boldsymbol{P}^T \boldsymbol{L}_\varepsilon \boldsymbol{N}_u \boldsymbol{u}_e + \frac{\delta q_i q_i}{b_{33} A_i^2} \right] \mathrm{d}V \, \mathrm{d}t = \int_{t_0}^{t} \left\{ \int_V \delta \boldsymbol{u}_e^T \boldsymbol{N}_u^T \boldsymbol{L}_u^T \boldsymbol{f}_B \, \mathrm{d}V \right.$$

$$\left. + \int_S \delta \boldsymbol{u}_e^T \boldsymbol{N}_u^T \boldsymbol{L}_u^T \boldsymbol{f}_S \, \mathrm{d}S + \sum_{i=1}^{n} \delta q_i \phi_i \right\} \mathrm{d}t \tag{20}$$

Note that only n degrees of freedom are added to the system, regardless of the discretization of the mechanical displacements. Integrating over the volume yields gives the governing equations for the coupled theory:

$$\delta\Pi_u = \delta \boldsymbol{u}_e^T \int_{t_0}^{t} (-\boldsymbol{M}_u \ddot{\boldsymbol{u}}_e - \boldsymbol{K}_{uu}\boldsymbol{u}_e - \boldsymbol{K}_{uq}\boldsymbol{q} + \boldsymbol{F}_u)\,\mathrm{d}t = 0 \quad (21a)$$

$$\delta\Pi_q = \delta \boldsymbol{q}^T \int_{t_0}^{t} (-\boldsymbol{K}_{qu}\boldsymbol{u}_e - \boldsymbol{K}_{qq}\boldsymbol{q} + \boldsymbol{F}_q)\,\mathrm{d}t = 0 \quad (21b)$$

where $\boldsymbol{q}$ is the vector of the PZT charges, $\boldsymbol{M}_u$ is the structural mass matrix, and $\boldsymbol{C}_u$ is the structural damping matrix. The matrix $\boldsymbol{K}_{uu}$ is the mechanical stiffness matrix, $\boldsymbol{K}_{qq}$ is the electrical stiffness matrix, and $\boldsymbol{K}_{uq}$ and $\boldsymbol{K}_{qu}$ are the stiffness matrices due to piezoelectric–mechanical coupling. The vectors $\boldsymbol{F}_u$ and $\boldsymbol{F}_q$ are the force vectors due to mechanical and electrical loading. These terms are further defined in the Appendix. To incorporate structural damping into the equations, a structural damping matrix $\boldsymbol{C}_u$ is added. The nature of the damping matrix can be chosen to meet the needs of the user. The governing equations can be written in matrix form as follows:

$$\begin{bmatrix} \boldsymbol{M}_u & \boldsymbol{0} \\ \boldsymbol{0} & \boldsymbol{0} \end{bmatrix} \begin{Bmatrix} \ddot{\boldsymbol{u}}_e \\ \ddot{\boldsymbol{q}} \end{Bmatrix} + \begin{bmatrix} \boldsymbol{C}_u & \boldsymbol{0} \\ \boldsymbol{0} & \boldsymbol{0} \end{bmatrix} \begin{Bmatrix} \dot{\boldsymbol{u}}_e \\ \dot{\boldsymbol{q}} \end{Bmatrix} + \begin{bmatrix} \boldsymbol{K}_{uu} & \boldsymbol{K}_{uq} \\ \boldsymbol{K}_{qu} & \boldsymbol{K}_{qq} \end{bmatrix} \begin{Bmatrix} \boldsymbol{u}_e \\ \boldsymbol{q} \end{Bmatrix} = \begin{Bmatrix} \boldsymbol{F}_u \\ \boldsymbol{F}_q \end{Bmatrix} \quad (22)$$

If the electric displacement has been discretized, then the equations of motion become

$$\sum_{i=1}^{n} \int_{t_0}^{t} \int_{V} \left[-\delta \boldsymbol{u}_e^T \boldsymbol{N}_u^T \boldsymbol{L}_\varepsilon^T \boldsymbol{P} \boldsymbol{B}^{-1} \begin{Bmatrix} 0 \\ 0 \\ 1 \end{Bmatrix} \boldsymbol{N}_q \left(\frac{\partial q_i}{\partial A} \right)_e \right.$$

$$- \delta \left(\frac{\partial q_i}{\partial A} \right)_e^T \boldsymbol{N}_q^T \begin{Bmatrix} 0 \\ 0 \\ 1 \end{Bmatrix}^T \boldsymbol{B}^{-1} \boldsymbol{P}^T \boldsymbol{L}_\varepsilon \boldsymbol{N}_u \boldsymbol{u}_e$$

$$\left. + \frac{1}{b_{33}} \delta \left(\frac{\partial q_i}{\partial A} \right)_e^T \boldsymbol{N}_q^T \boldsymbol{N}_q \left(\frac{\partial q_i}{\partial A} \right)_e \right] \mathrm{d}V\,\mathrm{d}t$$

$$+ \int_{t_0}^{t} \int_{V} \left[\delta \boldsymbol{u}_e^T \boldsymbol{N}_u^T \boldsymbol{L}_u^T \rho \boldsymbol{L}_u \boldsymbol{N}_u \ddot{\boldsymbol{u}}_e \right.$$

$$\left. + \delta \boldsymbol{u}_e^T \boldsymbol{N}_u^T \boldsymbol{L}_\varepsilon^T (\boldsymbol{Q} + \boldsymbol{P} \boldsymbol{B}^{-1} \boldsymbol{P}^T) \boldsymbol{L}_\varepsilon \boldsymbol{N}_u \boldsymbol{u}_e \right] \mathrm{d}V\,\mathrm{d}t$$

$$= \int_{t_0}^{t} \left\{ \int_{V} \delta \boldsymbol{u}_e^T \boldsymbol{N}_u^T \boldsymbol{L}_u^T \boldsymbol{f}_B\,\mathrm{d}V + \int_{S} \delta \boldsymbol{u}_e^T \boldsymbol{N}_u^T \boldsymbol{L}_u^T \boldsymbol{f}_S\,\mathrm{d}S \right.$$

$$\left. + \sum_{i=1}^{n} \int_{S} \delta \left(\frac{\partial q_i}{\partial A} \right)_e^T \boldsymbol{N}_q^T \phi_i\,\mathrm{d}S \right\} \mathrm{d}t \quad (23)$$

Integrating over the volume yields the governing equations for the coupled theory, which can be written in matrix form as follows:

$$\begin{bmatrix} \boldsymbol{M}_u & \boldsymbol{0} \\ \boldsymbol{0} & \boldsymbol{0} \end{bmatrix} \begin{Bmatrix} \ddot{\boldsymbol{u}}_e \\ \ddot{\boldsymbol{D}} \end{Bmatrix} + \begin{bmatrix} \boldsymbol{C}_u & \boldsymbol{0} \\ \boldsymbol{0} & \boldsymbol{0} \end{bmatrix} \begin{Bmatrix} \dot{\boldsymbol{u}}_e \\ \dot{\boldsymbol{D}} \end{Bmatrix} + \begin{bmatrix} \boldsymbol{K}_{uu} & \boldsymbol{K}_{uD} \\ \boldsymbol{K}_{Du} & \boldsymbol{K}_{DD} \end{bmatrix} \begin{Bmatrix} \boldsymbol{u}_e \\ \boldsymbol{D} \end{Bmatrix} = \begin{Bmatrix} \boldsymbol{F}_u \\ \boldsymbol{F}_D \end{Bmatrix} \quad (24)$$

where $\boldsymbol{D}$ is the vector of the PZT nodal electrical displacements. The stiffness matrices are further defined in the Appendix.

C. Electrical Equations

The absence of any electrical inertia or damping terms in Eqs. (22) and (24) is a result of only considering the mechanical aspects of the smart structure. When considering a smart structure as a whole, additional terms must be added for electrical components in the system. For a simple *LRC* circuit, the variational energy must include the following:

$$\delta\Pi_q = \delta\left(\tfrac{1}{2} L \dot{q}^2\right) - \delta q R \dot{q} - \delta[(1/2C)q^2] + V\delta q \quad (25)$$

where L, R, and C are the inductance, resistance, and capacitance and V is the applied voltage. The importance of formulating Hamilton's principle in terms of the charge, rather than electric field or potential, now becomes apparent. If the equations of motion for any electrical system attached to the smart structure can be formulated in the form

$$\boldsymbol{M}_q \ddot{\boldsymbol{q}}_e + \boldsymbol{C}_q \dot{\boldsymbol{q}}_e + \boldsymbol{K}_q \boldsymbol{q}_e = \boldsymbol{F}_q \quad (26)$$

then these equations can be directly combined with Eq. (22). This combination results in a completely coupled electrical–mechanical system of the form

$$\begin{bmatrix} \boldsymbol{M}_u & \boldsymbol{0} \\ \boldsymbol{0} & \boldsymbol{M}_q \end{bmatrix} \begin{Bmatrix} \ddot{\boldsymbol{u}}_e \\ \ddot{\boldsymbol{q}}_e \end{Bmatrix} + \begin{bmatrix} \boldsymbol{C}_u & \boldsymbol{0} \\ \boldsymbol{0} & \boldsymbol{C}_q \end{bmatrix} \begin{Bmatrix} \dot{\boldsymbol{u}}_e \\ \dot{\boldsymbol{q}}_e \end{Bmatrix} + \begin{bmatrix} \boldsymbol{K}_{uu} & \boldsymbol{K}_{uq} \\ \boldsymbol{K}_{qu} & \boldsymbol{K}_{qq}^* \end{bmatrix} \begin{Bmatrix} \boldsymbol{u}_e \\ \boldsymbol{q}_e \end{Bmatrix} = \begin{Bmatrix} \boldsymbol{F}_u \\ \boldsymbol{F}_q \end{Bmatrix} \quad (27)$$

where $\boldsymbol{q}_e$ includes not only the charge associated with the PZTs, but also the electrical system. Matrix $\boldsymbol{K}_{qq}^*$ also includes the electrical stiffness components of both the PZTs and the electrical system. If the electric displacement was discretized, then it is necessary to use the following relation between the electric displacement and the total PZT charge:

$$q_i = \left(\int_S \boldsymbol{N}_q\,\mathrm{d}S \right) \boldsymbol{D}_{i\,e} \qquad \text{or} \qquad \boldsymbol{q} = \boldsymbol{A}_q \boldsymbol{D}_e \quad (28)$$

When Eqs. (24) and (26) are combined, the resulting coupled electrical–mechanical system equations are obtained:

$$\begin{bmatrix} \boldsymbol{M}_u & \boldsymbol{0} \\ \boldsymbol{0} & \boldsymbol{A}_q^T \boldsymbol{M}_q \boldsymbol{A}_q \end{bmatrix} \begin{Bmatrix} \ddot{\boldsymbol{u}}_e \\ \ddot{\boldsymbol{D}}_e \end{Bmatrix} + \begin{bmatrix} \boldsymbol{C}_u & \boldsymbol{0} \\ \boldsymbol{0} & \boldsymbol{A}_q^T \boldsymbol{C}_q \boldsymbol{A}_q \end{bmatrix} \begin{Bmatrix} \dot{\boldsymbol{u}}_e \\ \dot{\boldsymbol{D}}_e \end{Bmatrix}$$

$$+ \begin{bmatrix} \boldsymbol{K}_{uu} & \boldsymbol{K}_{uD} \\ \boldsymbol{K}_{Du} & \boldsymbol{K}_{DD} + \boldsymbol{A}_q^T \boldsymbol{K}_q \boldsymbol{A}_q \end{bmatrix} \begin{Bmatrix} \boldsymbol{u}_e \\ \boldsymbol{D}_e \end{Bmatrix} = \begin{Bmatrix} \boldsymbol{F}_u \\ \boldsymbol{F}_D \end{Bmatrix} \quad (29)$$

Equations (27) and (29) provide the means to solve a variety of coupled piezoelectric–mechanical problems. The eigenvalues and eigenvectors can be determined to compute the natural frequencies and mode shapes of the system. The complex linear problem can be solved to determine the forced response of the system to a harmonic excitation. Systems with nonlinear components can be solved by using a time integration scheme, such as a fourth-order Runge–Kutta method. Thus, the system response for structures with semipassive damping using diodes for continuous switching of the PZTs, as proposed by Richard et al.,[16] can be modeled. Another advantage of this model is that the integration of the structural finite element model and electrical components allows for design of passive damping circuits for complicated structures using multivariable optimization methods. This technique would allow determination of optimum PZT location, orientation, and the electrical component values for single- or multimode damping of the structure.

D. System Reduction

Often it is desired to reduce a system using the mode shapes rather than work with the full finite element model. This drastically reduces the number of degrees of freedom and allows for much faster computations once the eigensystem is solved for. This is often done in structural mechanics because the necessary assumption that the modal matrix Φ uncouples the damping matrix $\boldsymbol{C}$ is usually valid for structural damping. That is,

$$\boldsymbol{\Phi}^T \boldsymbol{C} \boldsymbol{\Phi} = \mathrm{diag}[\mu_1 \quad \mu_2 \quad \cdots \quad \mu_m] \quad (30)$$

However, this assumption cannot be made for most electrical systems that would be connected to the PZTs. Therefore, in general, the coupled electrical–mechanical system of Eq. (27) could not be reduced in its entirety using a few of its mode shapes.

The system can be partially reduced using the structural mode shapes if the assumption is made that the mode shapes for the actual coupled system can be expressed in terms of the open circuit mode shapes. This assumption is generally very reasonable because changes in the elastic stiffness of PZTs due to open circuiting or short circuiting cause only modest shifts in natural frequency and very small alterations in the mode shapes. The structural stiffness added by the PZTs is generally small compared to the stiffness of the base structure, and the difference between open circuit and short circuit stiffness is only around 20%. This combined with the fact that PZTs usually only cover a fraction of the structural surface means that the differences in mode shapes between the open circuited condition and the actual structure will be generally small and localized.

First, the coupled system is reduced so that the open circuit eigenvalue problem can be solved for the desired number of eigenvalues:

$$\boldsymbol{K}_{uu}\varphi = \omega_{oc}^2 \boldsymbol{M}_u \varphi \tag{31}$$

Then, by use of Eq. (30) and

$$\Phi^T \boldsymbol{K}_{uu} \Phi = \operatorname{diag}\left[\omega_{oc1}^2 \quad \omega_{oc2}^2 \quad \cdots \quad \omega_{ocm}^2\right] \tag{32}$$

$$\Phi^T \boldsymbol{M}_u \Phi = \boldsymbol{I}_m \tag{33}$$

the coupled system of Eq. (33) can be reduced to

$$\begin{bmatrix} \boldsymbol{I}_m & \boldsymbol{0} \\ \boldsymbol{0} & \boldsymbol{M}_q \end{bmatrix} \begin{Bmatrix} \ddot{\boldsymbol{r}} \\ \ddot{\boldsymbol{q}}_e \end{Bmatrix} + \begin{bmatrix} \operatorname{diag}[\mu_m] & \boldsymbol{0} \\ \boldsymbol{0} & \boldsymbol{C}_q \end{bmatrix} \begin{Bmatrix} \dot{\boldsymbol{r}} \\ \dot{\boldsymbol{q}}_e \end{Bmatrix} + \begin{bmatrix} \operatorname{diag}\left[\omega_m^2\right] & \Phi^T \boldsymbol{K}_{uq} \\ \boldsymbol{K}_{qu}\Phi & \boldsymbol{K}_{qq}^* \end{bmatrix} \begin{Bmatrix} \boldsymbol{r} \\ \boldsymbol{q}_e \end{Bmatrix} = \begin{Bmatrix} \Phi^T \boldsymbol{F}_u \\ \boldsymbol{F}_q \end{Bmatrix} \tag{34}$$

where

$$\boldsymbol{r} = \Phi^{-1} \boldsymbol{u}_e \tag{35}$$

Now the problem has been reduced to a small system composed of only the electrical degrees of freedom and the chosen number of mode shapes.

III. Results

The model is verified by analysis of a structure with passive shunt damping. A cantilevered plate with shunt damping studied by Hagood and Von Flotow[1] is used. The aluminum plate seen in Fig. 2 has two pairs of PZTs mounted on the upper and lower surfaces. One pair is actuated in opposite directions to drive the vibration of the plate, and the other is connected to an inductor and resistor in series. The material properties of the plate and PZTs are listed in Table 1. This model is chosen for verification because the electrical system is relatively simple, but more important because of the availability of experimental data available in the literature.

Table 1 Material properties for cantilevered plate

Material property	Aluminum	PZT
E, GPa	73.0	63.0
ν	0.33	0.3[a]
ρ, kg/m^3	2800[a]	7750[a]
d_{31}, m/V	n/a	180×10^{-12}
e_3^S, F/m	n/a	9.22×10^{-9}

[a]Assumed values.

The cantilevered plate was modeled with a 28×3 finite element mesh. The higher-order laminate theory results in 8 degrees of freedom per node and 928 degrees of freedom total. The charge across the four PZT patches was described by four additional degrees of freedom. The open circuit mass matrix $\boldsymbol{M}_{uu}$ and stiffness matrix $\boldsymbol{K}_{uu}$ are used to solve for the first 12 open circuit modes with a LAPACK generalized eigensolver. The system is then reduced using Eq. (34) to determine the frequency response. The electrical equations for the each circuit are now added directly to the resulting set of equations. To create the damping matrix, 1% damping was assumed for each mode.

The model is first analyzed using an untuned shunt circuit containing only a resistor and no inductor. The increase in the damping coefficient ξ for the first bending mode is then calculated for a variety of resistance values. These results are shown in Fig. 3 against the nondimensional resistance. The nondimensional resistance is the ratio of the actual resistance to the optimum value of 28.68 kΩ predicted by Hagood and Von Flotow.[1] The results show good correlation with the published experimental values. Because the structural damping of the beam with the PZTs shorted out was only 0.16%, the untuned shunt damping circuit can be seen to roughly quadruple the damping of the structural system.

The plate is then modeled with a tuned shunt damping circuit. The inductor used has the optimum value of 148.2 H predicted by the literature.[1] It is connected in series with a resistor having a varying amount of resistance. Figure 4 shows the first bending mode frequency response for the plate with three conditions for the shunted PZTs: open circuited, shorted out, and optimally damped using the values of Hagood and Von Flowtow.[1] The results clearly show the reduction in natural frequency caused by shorting out the PZT. Also Fig. 4 shows how efficient the tuned damping circuit can be at damping out a particular mode of vibration. The frequency response for

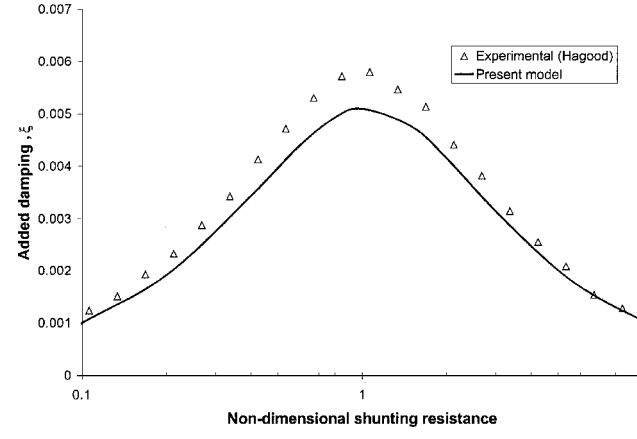

Fig. 3 Added damping to first mode of the cantilevered plate for untuned resistance shunting.

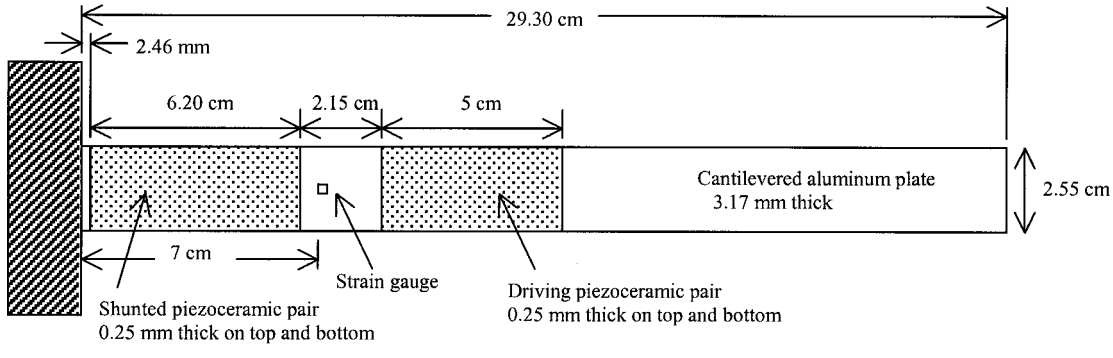

Fig. 2 Top view of cantilevered plate with driving and shunted piezoceramic pairs.

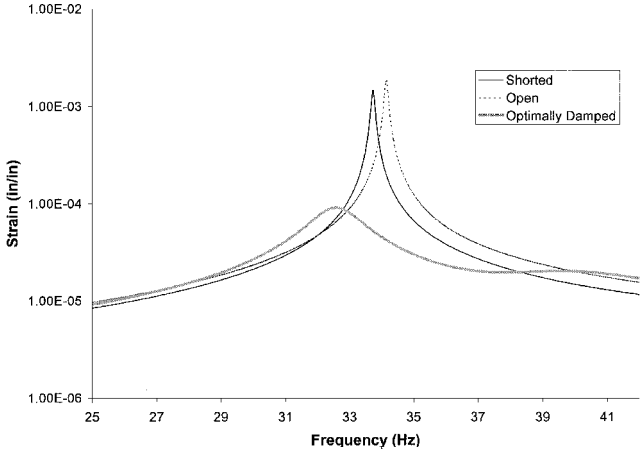

Fig. 4 Analytical strain for first mode actuation of cantilevered plate with shunted piezoceramic pair open, shunted, and optimally tuned and damped.

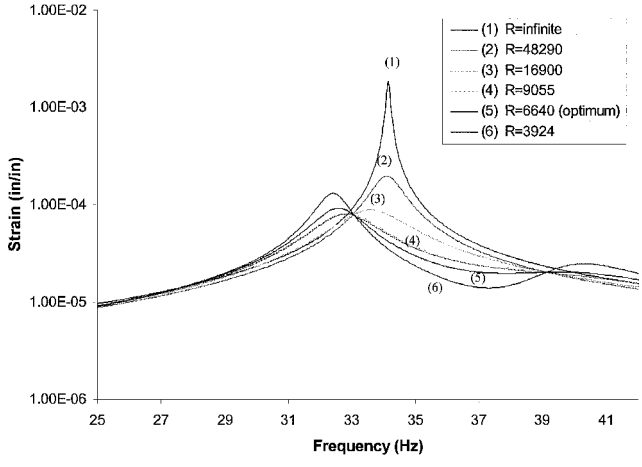

Fig. 5 Analytical strain for first mode actuation of cantilevered plate with tuned shunt circuit and varying resistance.

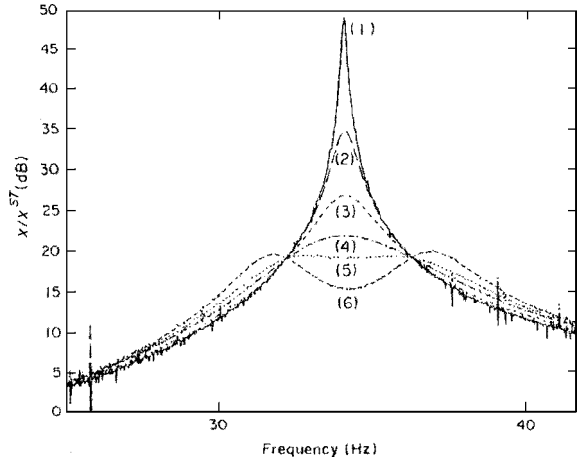

Fig. 6 Hagood and Von Flotow's experimental results[1] for first mode actuation of cantilevered plate with tuned shunt circuit and varying resistance.

the first mode is also shown in Fig. 5 for varying resistance. When the resistance is infinitely large, the system behaves as in open case. As resistance decreases, the damping increases, flattening the system response. As resistance decreases below the optimum value of 6640 Ω, the system begins to develop two separate peaks. These results show fair correlation with the experimental data of Hagood and Von Flotow[1] presented in Fig. 6; however, there are still noticeable differences. This is most likely the result of inaccuracy in the predicted natural frequency of the current theory. The finite element

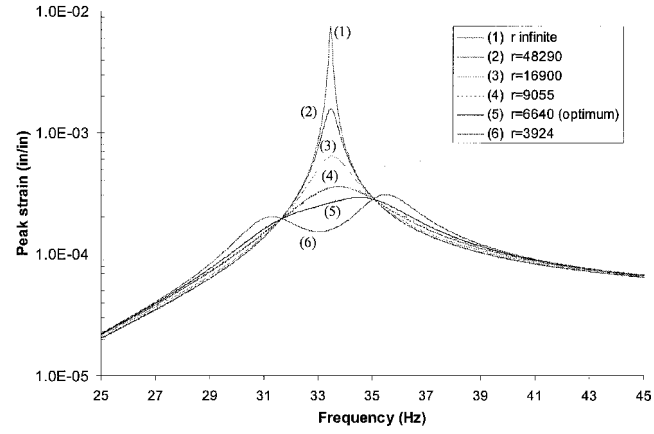

Fig. 7 Strain for first mode actuation of the modified cantilevered plate with tuned shunt circuit and varying resistance.

model predicts an open circuit natural frequency of 34.136 Hz as opposed to the measured natural frequency of 33.77 Hz. This is most likely caused by a combination of the finite element discretization, difference between the assumed material properties and the actual properties, and that electric displacement is assumed constant over the PZTs. When the finite element model is modified using lower stiffnesses to match closely the experimental value of natural frequency, the frequency responses are almost identical to the experimental results of Hagood and Von Flotow,[1] as shown in Fig. 7.

Next the multimode damping technique of Wu[6] is used on the same cantilevered aluminum plate. When a single mode is damped, an inductor and a resistor in parallel are connected to the shunted PZTs. This leads to electrical equations of the form

$$\begin{bmatrix} L & -L \\ -L & L \end{bmatrix} \ddot{\boldsymbol{q}} + \begin{bmatrix} 0 & 0 \\ 0 & R \end{bmatrix} \dot{\boldsymbol{q}} + \begin{bmatrix} 0 & 0 \\ 0 & 0 \end{bmatrix} \boldsymbol{q} = \begin{Bmatrix} 0 \\ 0 \end{Bmatrix} \tag{36}$$

where L and R are the inductance and resistance, respectively. These are then added to the structural finite element equations. The values of the inductance and resistance, determined using the method proposed by Wu,[6] are 199.4 H/113.7 kΩ, 8.888 H/27.66 kΩ, and 1.188 H/16.38 kΩ for bending modes 1, 2, and 3, respectively. The tip deflection as a function of frequency for the plate with mode 2 damped is plotted in Fig. 8 with that of the shorted plate. Next, modes 1 and 2 are damped with the circuit shown in Fig. 9. The values of L_2' and C_2' are chosen such that $L_2'C_2' = 1/\omega_1^2$ and are assumed to be 22.516 H and 1.00 μF, respectively. The values of R_2'' and L_2'', calculated using the multimode theory of Wu,[6] are 36.54 kΩ and 9.862 H, respectively. This leads to the electrical equations given by

$$\begin{bmatrix} 0 & 0 & 0 & 0 & 0 \\ 0 & 0 & 0 & 0 & 0 \\ 0 & 0 & L_1 & 0 & 0 \\ 0 & 0 & 0 & L_2' & 0 \\ 0 & 0 & 0 & 0 & L_2'' \end{bmatrix} \ddot{\boldsymbol{q}} + \begin{bmatrix} R_1 & -R_1 & -R_1 & 0 & 0 \\ -R_1 & R_1 + R_2'' & R_1 & 0 & -R_2'' \\ -R_1 & R_1 & R_1 & 0 & 0 \\ 0 & 0 & 0 & 0 & 0 \\ 0 & -R_2'' & 0 & 0 & R_2'' \end{bmatrix} \dot{\boldsymbol{q}}$$

$$+ \begin{bmatrix} 0 & 0 & 0 & 0 & 0 \\ 0 & 1/C_2' & 0 & -1/C_2' & 0 \\ 0 & 0 & 0 & 0 & 0 \\ 0 & -1/C_2' & 0 & 1/C_2' & 0 \\ 0 & 0 & 0 & 0 & 0 \end{bmatrix} \boldsymbol{q} = \begin{Bmatrix} 0 \\ 0 \\ 0 \\ 0 \\ 0 \end{Bmatrix} \tag{37}$$

The resulting frequency response is shown in Fig. 10. This technique can be seen to result in a decrease in maximum tip deflection of over one order of magnitude. This versatile technique can also be extended to as many modes as one wishes to damp out.

Finally, a comparison is made between the open circuited and short circuited mode shapes. As already discussed, the system can be reduced using its open circuited eigenvectors. However, it is

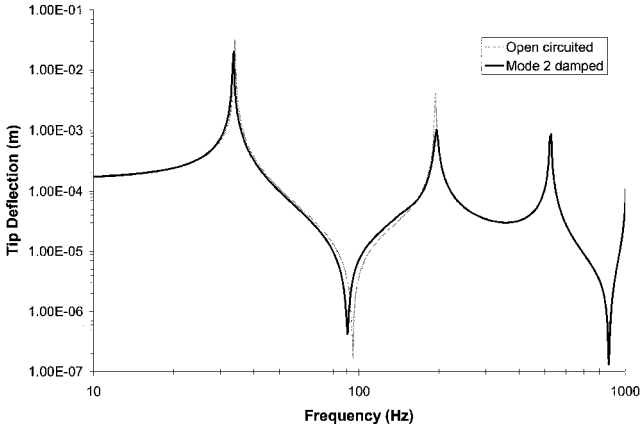

Fig. 8 Frequency response for aluminum plate with mode 2 damped.

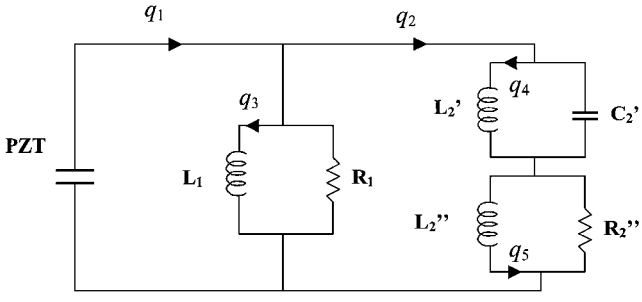

Fig. 9 Two-mode damping circuit.

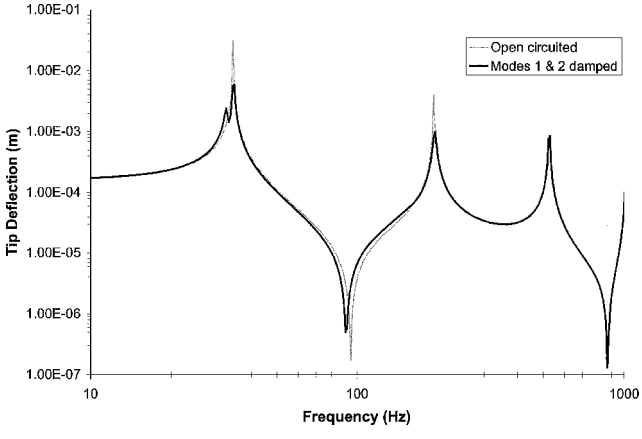

Fig. 10 Frequency response for aluminum plate with modes 1 and 2 damped.

desirable to estimate the nature of any resulting errors when this technique is applied to an electrical system where the short circuit mode shapes are more appropriate. Because the open and shorted eigenvectors are both normalized to the same mass matrix, the difference between the two can be directly calculated. Then to compare the deviation, the norm of the difference can be compared to the norm of the original eigenvector. The ratio of the 2-norms of the difference to the open circuit mode shape is found to be 1.79×10^{-5}, 4.53×10^{-5}, and 2.73×10^{-5} for the first three bending modes of the cantilevered aluminum plate used earlier. These very small differences are negligible when compared to the changes in natural frequency, which are on the order of 1%. Thus, the technique for using open circuit mode shapes for system reduction will likely yield good results in most practical problems.

IV. Conclusions

A smart structural model was developed that is capable of simultaneously modeling the electrical and mechanical response of arbitrary structures with piezoelectric materials and attached electrical circuitry. The equations of motion were formulated using the coupled piezoelectric equations, but the solution solves for the strain and electric charge, as opposed to strain and electric field used in most formulations. A method was also presented for system simplification using mode shapes and natural frequencies of the open circuit structural system. Application of the model was shown for a cantilever plate with passive electrical shunt damping with several electrical circuits, including a multiple mode damping circuit, with good correlation to experimental data. The developed model results has the following advantages over other models:

1) The framework for this model is general and can be applied to classical, higher-order, and layerwise plate and shell theories.

2) Electrical charge is inherently conserved across piezoelectric elements resulting in more accurate solutions.

3) Piezoelectric charge can be modeled with only one additional degree of freedom per PZT or meshed across a PZT to capture the effects of stress gradients.

4) Simultaneous solutions of both structural and electrical components allow modeling of a wide variety of coupled piezoelectric–mechanical problems such as passive electrical damping, self-sensing, and electrical power consumption.

Appendix: Definitions

The following are the definitions for the matrices in Eqs. (22) and (24):

$$\boldsymbol{M}_u = \int_{A_e}\int_{-h/2}^{h/2} \boldsymbol{N}_u^T \boldsymbol{L}_u^T \rho \boldsymbol{L}_u \boldsymbol{N}_u \,\mathrm{d}z\,\mathrm{d}A \tag{A1}$$

$$\boldsymbol{K}_{uu} = \int_{A_e}\int_{-h/2}^{h/2} \boldsymbol{N}_u^T \boldsymbol{L}_\varepsilon^T (\boldsymbol{Q} + \boldsymbol{P}\boldsymbol{B}^{-1}\boldsymbol{P}^T) \boldsymbol{L}_\varepsilon \boldsymbol{N}_u \,\mathrm{d}z\,\mathrm{d}A \tag{A2}$$

$$\boldsymbol{K}_{uq} = \left[-\int_{A_e}\int_{zL_1}^{zu_1} \boldsymbol{N}_u^T \boldsymbol{L}_\varepsilon^T \boldsymbol{P}_1 \boldsymbol{B}_1^{-1} \begin{Bmatrix} 0 \\ 0 \\ 1 \end{Bmatrix} \frac{1}{A_1} \,\mathrm{d}z\,\mathrm{d}A, \ldots, \right.$$

$$\left. -\int_{A_e}\int_{zL_m}^{zu_m} \boldsymbol{N}_u^T \boldsymbol{L}_\varepsilon^T \boldsymbol{P}_m \boldsymbol{B}_m^{-1} \begin{Bmatrix} 0 \\ 0 \\ 1 \end{Bmatrix} \frac{1}{A_m} \,\mathrm{d}z\,\mathrm{d}A \right] \tag{A3}$$

where m is the number of PZTs. Also,

$$\boldsymbol{K}_{qu} = \boldsymbol{K}_{uq}^T \tag{A4}$$

$$\boldsymbol{K}_{qq} = \begin{bmatrix} \dfrac{1}{(b_{33})_1 A_1} & \cdots & 0 \\ \cdots & \cdots & \cdots \\ 0 & \cdots & \dfrac{1}{(b_{33})_m A_m} \end{bmatrix} \tag{A5}$$

$$\boldsymbol{K}_{uD} = \left[-\int_{A_e}\int_{zL_1}^{zu_1} \boldsymbol{N}_u^T \boldsymbol{L}_\varepsilon^T \boldsymbol{P}_1 \boldsymbol{B}_1^{-1} \begin{Bmatrix} 0 \\ 0 \\ 1 \end{Bmatrix} (\boldsymbol{N}_q)_1 \,\mathrm{d}z\,\mathrm{d}A, \ldots, \right.$$

$$\left. -\int_{A_e}\int_{zL_m}^{zu_m} \boldsymbol{N}_u^T \boldsymbol{L}_\varepsilon^T \boldsymbol{P}_m \boldsymbol{B}_m^{-1} \begin{Bmatrix} 0 \\ 0 \\ 1 \end{Bmatrix} (\boldsymbol{N}_q)_m \,\mathrm{d}z\,\mathrm{d}A \right] \tag{A6}$$

$$\boldsymbol{K}_{Du} = \boldsymbol{K}_{uD}^T \tag{A7}$$

$$\boldsymbol{K}_{DD} = \begin{bmatrix} \displaystyle\int_{A_e} \frac{1}{(b_{33})_1} \left(\boldsymbol{N}_q^T\right)_1 (\boldsymbol{N}_q)_1 \,\mathrm{d}A & \cdots & 0 \\ \cdots & \cdots & \cdots \\ 0 & \cdots & \displaystyle\int_{A_e} \frac{1}{(b_{33})_m} \left(\boldsymbol{N}_q^T\right)_m (\boldsymbol{N}_q)_m \,\mathrm{d}A \end{bmatrix} \tag{A8}$$

$$\boldsymbol{F}_u = \int_{A_e}\int_{-h/2}^{h/2} \boldsymbol{N}_u^T \boldsymbol{L}_u^T f_B \,\mathrm{d}z\,\mathrm{d}A + \int_{A_e} \boldsymbol{N}_u^T \boldsymbol{L}_u^T f_S \,\mathrm{d}A \tag{A9}$$

$$\boldsymbol{F}_q = \begin{bmatrix} \phi_1 \\ \vdots \\ \phi_m \end{bmatrix} \tag{A10}$$

$$\boldsymbol{F}_D = \begin{bmatrix} \int_{A_e} \left(\boldsymbol{N}_q^T\right)_1 \phi_1 \, \mathrm{d}A \\ \vdots \\ \int_{A_e} \left(\boldsymbol{N}_q^T\right)_m \phi_m \, \mathrm{d}A \end{bmatrix} \tag{A11}$$

Acknowledgments

The authors would like to thank Mercedes Reaves and Lucas Horta of the Structural Dynamics Branch at NASA Langley Research Center whose support via the Langley Research Summer Scholars Program made this research possible.

References

[1]Hagood, N. W., and Von Flotow, A., "Damping of Structural Vibrations with Piezoelectric Materials and Passive Electrical Networks," *Journal of Sound and Vibration*, Vol. 146, No. 2, 1991, pp. 243–268.

[2]Hagood, N. W., and Crawley, E. F., "Experimental Investigation of Passive Enhancement of Damping for Space Structures," *Journal of Guidance, Control, and Dynamics*, Vol. 14, No. 6, 1991, pp. 1100–1009.

[3]Agnes, G. S., "Active/Passive Piezoelectric Vibration Suppression," *Smart Structures and Materials 1994: Passive Damping*, edited by C. D. Johnson, Proceedings of the SPIE 2193, Society of Photo-Optical Instrumentation Engineers—The International Society of Optical Engineering, Bellingham, WA, 1994, pp. 24–34.

[4]Wu, S. Y., "Piezoelectric Shunts with a Parallel R-L Circuit for Structural Damping and Vibration Control," *Smart Structures and Materials 1996: Passive Damping*, edited by C. D. Johnson, Proceedings of the SPIE 2720, Society of Photo-Optical Instrumentation Engineers—The International Society of Optical Engineering, Bellingham, WA, 1996, pp. 259–269.

[5]Wu, S. Y., and Bicos, A. S., "Structural Vibration Damping Experiments Using Improved Piezoelectric Shunts," *Smart Structures and Materials 1997: Passive Damping and Isolation*, edited by L. Davis, Proceedings of the SPIE 3045, Society of Photo-Optical Instrumentation Engineers—The International Society of Optical Engineering, Bellingham, WA, 1997, pp. 40–50.

[6]Wu, S. Y., "Method for Multiple Mode Shunt Damping of Structural Vibration Using a Single PZT Transducer," *Smart Structures and Materials 1998: Passive Damping and Isolation*, edited by L. Davis, Proceedings of the SPIE 3327, Society of Photo-Optical Instrumentation Engineers—The International Society of Optical Engineering, Bellingham, WA, 1998, pp. 112–122.

[7]Anderson, E. H., and Hagood, N. W., "Simultaneous Piezoelectric Sensing/Actuation: Analysis and Application to Controlled Structures," *Journal of Sound and Vibration*, Vol. 174, No. 5, 1994, pp. 617–639.

[8]Crawley, E. F., "Use of Piezoelectric Actuators as Elements of Intelligent Structures," *AIAA Journal*, Vol. 25, No. 10, 1987, pp. 1373–1385.

[9]Detwiler, D. T., Shen, M. H., and Venkayya, V. B., "Finite Element Analysis of Laminated Composite Structures Containing Distributed Piezoelectric Actuators and Sensors," *Finite Elements in Analysis and Design*, Vol. 20, No. 2, 1995, pp. 87–100.

[10]Mitchell, J. A., and Reddy, J. N., "A Refined Hybrid Plate Theory for Composite Laminates with Piezoelectric Laminae," *International Journal of Solids and Structures*, Vol. 32, No. 16, 1995, pp. 2345–2367.

[11]Chattopadhyay, A., Li, J., and Gu, H., "Coupled Thermo-Piezoelectric–Mechanical Model for Smart Composite Laminates," *AIAA Journal*, Vol. 37, No. 12, 1999, pp. 1633–1638.

[12]Zhou, X., Chattopadhyay, A., and Thornburgh, R. P., "Analysis of Piezoelectric Smart Composites Using a Coupled Piezoelectric-Mechanical Model," *Journal of Intelligent Material Systems and Structures*, Vol. 11, No. 3, 2000, pp. 169–179.

[13]Tiersten, H. F., "Hamilton's Principle for Linear Piezoelectric Media," *IEEE Proceedings*, Vol. 55, No. 8, 1967, pp. 1523, 1524.

[14]Reddy, J. N., "A Simple Higher-Order Theory for Laminated Composite Plates," *Journal of Applied Mechanics*, Vol. 51, 1984, pp. 745–752.

[15]Reddy, J. N., *Mechanics of Laminated Composite Plates: Theory and Analysis*, CRC Press, Boca Raton, FL, 1997, pp. 599–603.

[16]Richard, C., Guyomar, D., Audigier, D., and Ching, G., "Semi-Passive Damping Using Continuous Switching of a Piezoelectric Device," *Smart Structures and Materials 1999: Passive Damping and Isolation*, edited by T. Hyde, Proceedings of the SPIE 3672, Society of Photo-Optical Instrumentation Engineers—The International Society of Optical Engineering, Bellingham, WA, 1999, pp. 104–111.

A. M. Baz
Associate Editor